



NON-LINEAR TRANSIENT RESPONSE OF FLUTTERING STIFFENED COMPOSITE PLATES SUBJECT TO THERMAL LOAD

I. K. OH AND I. LEE

Department of Aerospace Engineering, Korea Advanced Institute of Science and Technology, 373-1 Kusong-Dong, Yusong-Gu, Taejon 305-701, South Korea. E-mail: inlee@asdl.kaist.ac.kr

AND

D. M. LEE

Agency for Defense Development, Taejon, South Korea

(Received 26 July 2000, and in final form 17 January 2001)

Non-linear transient response of fluttering stiffened composite plates subject to thermal loads has been analyzed. The first order shear deformable plate and Timoshenko beam theories are used for the finite element modelling of a skin panel and stiffeners considering von Karman non-linear strain–displacement relationships. A supersonic piston theory is used for modelling aerodynamic loads. In order to find a critical flutter speed, linear flutter analysis of stiffened laminated panels considering large aero-thermal deflections has been performed. The flat and stable motion, limit cycle oscillation, and buckled but dynamically stable and chaotic motion of stiffened laminated panels have been investigated using the implicit Newmark integration method. Results show that the increase of the height and number of stiffeners to reduce an aero-thermal deflection can dramatically drop the boundaries of a dynamic stability at a certain point. Also, the non-linear behaviors, such as dynamically stable motions with static aero-thermal deflections, limit cycle oscillations, periodic motions with large amplitude and chaotic oscillations, are observed in the time domain analysis.

© 2001 Academic Press

1. INTRODUCTION

It is well known that the structural design using stiffeners to enhance a static and dynamic stability is very efficient in structural engineering applications. Nowadays, stiffened composite panels have been extensively used in high-performance aerospace, naval and civil structures. Especially, aircraft and rockets in a supersonic regime are subject to severe aerodynamic and high thermal loads. While using stiffened laminated panels in these vehicles, static aero-thermal and aerothermoelastic analyses should precede, from the viewpoint of confirming static and dynamic stability of structural components.

An excellent review of the linear and non-linear panel flutter, including mathematical physics and experimental aspects, can be found in reference [1]. With respect to realistic physics, a fatigue failure of structures due to fluttering motions is always possible without a catastrophic failure. So the investigations of non-linear flutter characteristics as well as the flutter boundaries are very important prior to fatigue analysis. Because a direct time integration scheme for non-linear analysis requires a lot of time cost and additional labor for understanding the numerical results, the perturbation and harmonic balance methods

[2] and an incremental harmonic balance method [3] for non-linear panel flutter were developed. Also, using LUM/NTF frequency domain approach, Xue and Mei [4] reported the non-linear panel flutter of composite panels considering thermal effects. As a time domain scheme, Zhou *et al.* [5] and Abbas *et al.* [6] investigated non-linear flutter of panel under aerodynamic heating with mutual understanding of power spectra and time responses. Recently, Udrescu [7] studied the snap-through behavior of thermally buckled and fluttering panels with multiple equilibrium points. With respect to non-linear aerothermoelastic investigations, the use of both frequency and time domain approaches to make up for weak points is quite reasonable to fully understand non-linear characteristics of the panel flutter.

Unlike unstiffened panels, only a few studies on the flutter characteristics of stiffened laminated panels exist. Liao and Sun [8] investigated the linear flutter analysis of stiffened panels using the finite element method along with three-dimensional degenerated shell and curved elements. Lee and Lee [9] reported the linear supersonic flutter characteristics of stiffened laminated panels using finite elements based on the first order shear deformable plate and Timoshenko beam theories. They discussed the effects of lamination scheme, stiffener size, and flow angle on the flutter characteristics. Lee *et al.* [10] extended their previous works to non-linear flutter analyses of stiffened composite panels subject to thermal loads using a frequency domain technique.

In this study, as in a subsequent study of previous works [9, 10], the non-linear transient response of fluttering stiffened panels considering thermal effect is investigated. In order to find a critical flutter speed, linear flutter analysis of a stiffened laminated panel considering large aero-thermal deflections is performed. Non-linear fluttering motions, such as flat and stable motions, limit cycle oscillations, and buckled but dynamically stable and chaotic motions of stiffened laminated panels are investigated using the implicit Newmark integration method. Results show that the increase of the height and number of stiffeners to reduce an aero-thermal deflection can dramatically drop the boundaries of a dynamic stability at a certain point. Also, the non-linear characteristics, such as dynamically stable motions with static aero-thermal deflections, limit cycle oscillations, periodic motions with a large amplitude and chaotic motions, are observed in the time domain analysis.

2. FINITE ELEMENT EQUATIONS OF FLUTTERING STIFFENED PANELS

2.1. SKIN PLATE MODEL

The von Karman non-linear relationships between strain and displacement in FSDT are given as follows:

$$\{e\} = \{\varepsilon\} + z\{\kappa\} = \{\varepsilon_m\} + \{\varepsilon_\theta\} + z\{\kappa\}, \quad \{\gamma\} = \{\gamma_{yz} \quad \gamma_{xz}\}^T, \quad (1)$$

where

$$\{\varepsilon_m\} = \{u_{,x} \ v_{,y} \ u_{,y} + v_{,x}\}^T, \quad \{\varepsilon_\theta\} = \frac{1}{2}\{w_{,x}^2 \ w_{,y}^2 \ 2w_{,x} \ w_{,y}\}^T,$$

$$\{\kappa\} = \{\phi_{x,x} \ \phi_{y,x} \ \phi_{x,y} \ \phi_{y,x}\}^T, \quad \{\gamma\} = \{w_{,y} + \phi_y \quad w_{,x} + \phi_x\}^T.$$

Here, u , v , and w are the displacements in the x , y , and z direction, respectively; ϕ_x and ϕ_y are rotation in the xz - and yz -planes respectively. The comma and subscript denote the partial derivative with respect to the subscript.

For an anisotropic plate subjected to any temperature change $\Delta T(x, y, z)$, the well-known constitutive relationships can be obtained by integrating the stress-strain equations

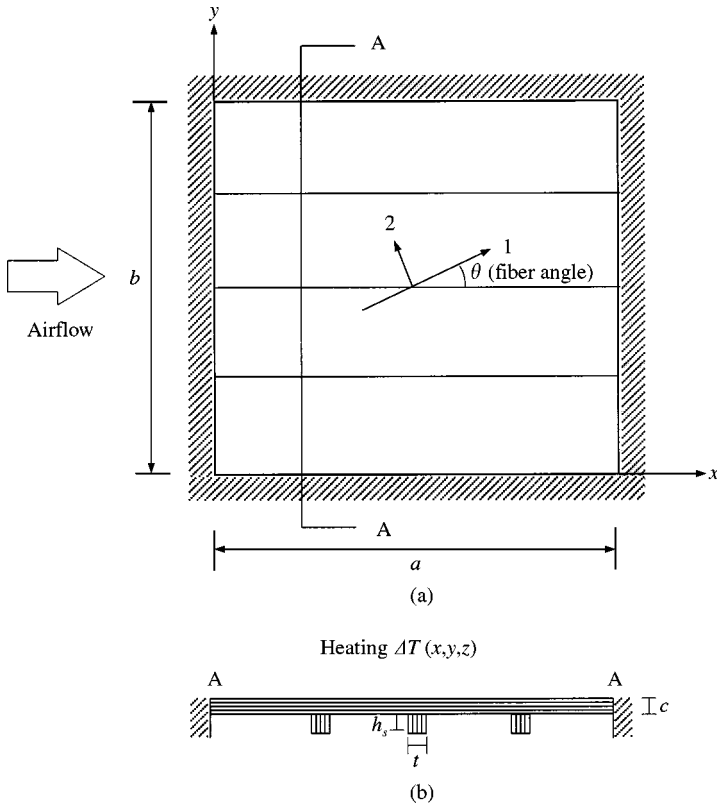


Figure 1. Schematic diagram of stiffened composite plate subject to aerodynamic and thermal loads. (a) Top view of panel; (b) section A-A.

through the thickness of plates as

$$\begin{Bmatrix} N \\ M \end{Bmatrix} = \begin{bmatrix} A & B \\ B & D \end{bmatrix} \begin{Bmatrix} \epsilon \\ \kappa \end{Bmatrix} - \begin{Bmatrix} N_{AT} \\ M_{AT} \end{Bmatrix}, \quad \{Q\} = \begin{Bmatrix} Q_{yz} \\ Q_{xz} \end{Bmatrix} = \begin{bmatrix} A_{44} & A_{45} \\ A_{45} & A_{55} \end{bmatrix} \{\gamma\}, \quad (2)$$

where $\{N\}$, $\{M\}$ and $\{Q\}$ are in-plane load, moment and transverse load vectors, respectively; the thermal in-plane load and moment vectors are given as

$$\left(\{N_{AT}\}, \{M_{AT}\} \right) = \sum_{k=1}^n \int_{z_{k-1}}^{z_k} [\bar{Q}]_k \{\bar{\alpha}\}_k (1, z) \Delta T dz. \quad (3)$$

2.2. STIFFENER MODEL

The Timoshenko beam theory is used for the modelling of anisotropic stiffeners along the x -axis as shown in Figure 1 satisfying the compatibility conditions between skin plate and stiffeners. The displacement fields of stiffeners are assumed as

$$u^b = u - e\phi_x + z\phi_x, \quad v^b = v + z\phi_y, \quad w^b = w - y\phi_y, \quad (4)$$

where the superscript b denotes the stiffener and e is the eccentricity of the stiffener defined as $e = \frac{1}{2}(c + h_s)$. The strain–displacement relationships can be given as follows:

$$\{e^b\} = \{e_m\} + \{e_n\} + \{e_r\}, \quad \gamma_{xy}^b = v_{,x} + z\phi_{y,x}, \quad (5)$$

where

$$\{e_m\} = \{u_{,x} - e\phi_{x,x} \quad \phi_x + w_{,x}\}^T, \quad \{e_n\} = 1/2\{w_{,x}^2 \ 0\}^T, \quad \{e_r\} = \{z\phi_{x,x} - y\phi_{y,x}\}^T.$$

Assuming that σ_y and σ_z are negligible due to the ratio between the width (or height) and the length along x -axis, we can obtain the constitutive equations for a stiffener as follows:

$$\begin{Bmatrix} \sigma_x^b \\ \tau_{xz}^b \end{Bmatrix} = \begin{bmatrix} C_{11} & C_{16} \\ C_{16} & C_{66} \end{bmatrix} \left(\begin{Bmatrix} e_x^b \\ \gamma_{xz}^b \end{Bmatrix} - \begin{Bmatrix} \alpha_x^b \\ \alpha_{xz}^b \end{Bmatrix} \Delta T \right), \quad \tau_{xy}^b = C_{55} \gamma_{xy}^b, \quad (6)$$

where the stiffness coefficients, C_{ij} , are called modified reduced stiffness and the relation between the stiffness coefficients can be referred to reference [11].

2.3. DERIVATION OF FINITE ELEMENT GOVERNING EQUATIONS

The equation of motion can be derived using Hamilton's principle as follows:

$$\begin{aligned} \delta\Pi &= \delta(U + V) - \delta K \\ &= \int_0^T \left\{ \int_V (\sigma_i \delta \varepsilon_i - f_i \delta u_i - \rho \dot{u}_i \delta \dot{u}_i) dV - \int_S T_i \delta u_i dS \right\} dt \\ &= 0. \end{aligned} \quad (7)$$

The non-linear finite element equation for each element can be obtained by the introduction of Lagrangian shape functions as follows:

$$\mathbf{M}_e \ddot{\mathbf{u}}_e + (\mathbf{K}_0 - \mathbf{K}_e^{AT} + \frac{1}{2} \mathbf{KN1}_e + \frac{1}{3} \mathbf{KN2}_e) \mathbf{u}_e = \mathbf{F}_e^{AT} + \mathbf{F}_e^{AP}, \quad (8)$$

where \mathbf{M}_e , \mathbf{K}_0 , \mathbf{K}_e^{AT} , $\mathbf{KN1}_e$, $\mathbf{KN2}_e$, \mathbf{F}_e^{AT} and \mathbf{F}_e^{AP} are mass matrix, linear stiffness, thermal geometric stiffness, first order non-linear stiffness, second order non-linear stiffness, thermal load vector and dynamic pressure force vectors respectively. The detailed expressions can be referred to in reference [10].

2.4. AERODYNAMIC LOAD MODEL

Based on the supersonic piston theory, the aerodynamic stiffness and damping matrices can be derived using the virtual work done by the aerodynamic load ΔP as follows:

$$\begin{aligned} \Delta P &= -\frac{2q}{\sqrt{M^2 - 1}} \left\{ \frac{\partial w}{\partial x} + \frac{1}{U_\infty} \left(\frac{M^2 - 2}{M^2 - 1} \right) \frac{\partial w}{\partial t} \right\} \\ &= -\beta \frac{\partial w}{\partial x} - g \frac{\partial w}{\partial t}, \end{aligned} \quad (9)$$

where β and g are the aerodynamic pressure parameter and damping parameter, respectively; w is the transverse deflection of skin panel. Here, one can obtain the aerodynamic force vector with respect to finite element nodal displacements as follows:

$$\mathbf{F}_e^{AP} = -\beta \mathbf{A}_\beta \mathbf{u}_e - g \mathbf{A}_g \dot{\mathbf{u}}_e. \quad (10)$$

Through the assembly procedure, the global finite element equation can be obtained as follows:

$$\mathbf{M}\ddot{\mathbf{u}} + g \mathbf{A}_g \dot{\mathbf{u}} + (\mathbf{K}\mathbf{0} + \beta \mathbf{A}_\beta - \mathbf{K}^{AT} + \frac{1}{2} \mathbf{K}\mathbf{N1} + \frac{1}{3} \mathbf{K}\mathbf{N2}) \mathbf{u} = \mathbf{F}^{AT}. \quad (11)$$

3. SOLUTION SCHEME FOR STIFFENED LAMINATED PANELS

3.1. LINEAR FLUTTER ANALYSIS CONSIDERING LARGE AERO-THERMAL DEFLECTION

In order to analyze the aerothermoelastic deformation and vibration of stiffened plates considering large deflections, the solution of equation (11) is assumed to be the sum of a time-dependent and a time-independent solution, $\mathbf{u} = \mathbf{u}_s + \mathbf{u}_t$, where \mathbf{u}_s is the static large deflection and \mathbf{u}_t is the time-dependent solution with small amplitude. Substituting this assumed displacement into equation (11), we can obtain static and dynamic coupled equations.

$$(\mathbf{K}\mathbf{0} + \beta \mathbf{A}_\beta - \mathbf{K}^{AT} + \frac{1}{2} \mathbf{K}\mathbf{N1}(\mathbf{u}_s) + \frac{1}{3} \mathbf{K}\mathbf{N2}(\mathbf{u}_s)) \mathbf{u}_s = \mathbf{F}^{AT}, \quad (12)$$

$$\mathbf{M}\ddot{\mathbf{u}}_t + g \mathbf{A}_g \dot{\mathbf{u}}_t + (\mathbf{K}\mathbf{0} + \beta \mathbf{A}_\beta - \mathbf{K}^{AT} + \mathbf{K}\mathbf{N1}(\mathbf{u}_s) + \mathbf{K}\mathbf{N2}(\mathbf{u}_s)) \mathbf{u}_t = \mathbf{0}. \quad (13)$$

Firstly, thermal Euler buckling analysis is performed to find the reference buckling temperature rise using the following equation:

$$(\mathbf{K}\mathbf{0} - \Delta T_{cr} \mathbf{K}_0^{AT}) \{\Theta\} = \mathbf{0}, \quad (14)$$

where \mathbf{K}_0^{AT} is the geometric stiffness in the state of unit uniform temperature distribution; ΔT_{cr} and $\{\Theta\}$ are the critical buckling temperature increase and the buckling mode shape respectively. The buckling mode shape is properly scaled as an initial estimated deflection in the construction of non-linear stiffness matrix in the postbuckled range.

The Newton–Raphson iteration method is used to solve the aerothermoelastic postbuckling problem. For the i th iteration, an incremental equation can be written from equation (12) as

$$(\mathbf{K}\mathbf{0} + \beta \mathbf{A}_\beta - \mathbf{K}^{AT} + \mathbf{K}\mathbf{N1}(\mathbf{u}_s^i) + \mathbf{K}\mathbf{N2}(\mathbf{u}_s^i)) \Delta \mathbf{u}_s^{i+1} = \Delta \mathbf{F}^i \quad (15)$$

where

$$\Delta \mathbf{F}^i = \mathbf{F}^{AT} - (\mathbf{K}\mathbf{0} + \beta \mathbf{A}_\beta - \mathbf{K}^{AT} + \frac{1}{2} \mathbf{K}\mathbf{N1}(\mathbf{u}_s^i) + \frac{1}{3} \mathbf{K}\mathbf{N2}(\mathbf{u}_s^i)) \mathbf{u}_s^i. \quad (16)$$

By solving equation (15), the updated displacement vector is determined as follows:

$$\mathbf{u}_s^{i+1} = \mathbf{u}_s^i + \Delta \mathbf{u}_s^{i+1} \quad (17)$$

where \mathbf{u}_s^{i+1} and $\Delta \mathbf{u}_s^{i+1}$ are the static and incremental displacement in the $(i + 1)$ th iteration.

Full system equations with skew symmetric aerodynamic matrix need very large d.o.f. and computational cost. In this study, the modal reduction is applied to find flutter speed. The reduced flutter equation using modal approach can be obtained by

$$\mathbf{M}^* \ddot{\mathbf{U}} + \mathbf{K}(\beta, \mathbf{u}_s)^* \mathbf{U} = \mathbf{0}, \quad (18)$$

where

$$\mathbf{M}^* = \Phi^T \mathbf{M} \Phi \quad (19)$$

$$\mathbf{K}(\beta, \mathbf{u}_s)^* = \Phi^T (\mathbf{K}\mathbf{0} + \beta \mathbf{A}_\beta - \mathbf{K}^{AT} + \mathbf{KN1}(\mathbf{u}_s) + \mathbf{KN2}(\mathbf{u}_s)) \Phi. \quad (20)$$

For a simple presentation of analysis results, the following non-dimensional parameters are introduced as

$$\beta^* = \beta \frac{a^3}{D}, \quad \bar{\omega}_i = \omega_i \sqrt{a^4 \frac{\rho c}{D}}, \quad (21)$$

where β^* and $\bar{\omega}_i$ are the non-dimensional dynamic pressure and frequencies, respectively; a and c are side length and thickness of skin panel, respectively; D is rigidity of panel ($D = Ec^3/12(1 - \nu^2)$ for isotropic material and $D = E_2c^3$ for anisotropic material).

3.2. IMPLICIT NEWMARK INTEGRATION SCHEME

The spatially discrete system of equation (11) to be solved at each time t may be written in terms of the displacement vector $\mathbf{u}(t)$ as

$$\mathbf{q}(\mathbf{u}) = \mathbf{M}\ddot{\mathbf{u}} + g\mathbf{A}_g\dot{\mathbf{u}} + (\mathbf{K}\mathbf{0} + \beta\mathbf{A}_\beta - \mathbf{K}^{AT} + \frac{1}{2}\mathbf{KN1} + \frac{1}{3}\mathbf{KN2})\mathbf{u} - \mathbf{F}^{AT} = \mathbf{0}, \quad (22)$$

where $\mathbf{q}(\mathbf{u})$ is the n -dimensional residual vector. In Newmark's method, the approximate displacement and velocity are given as

$$\begin{aligned} \dot{\mathbf{u}}_{n+1} &= \dot{\mathbf{u}}_n + (1 - \alpha)h\ddot{\mathbf{u}}_n + \alpha h\ddot{\mathbf{u}}_{n+1}, \\ \mathbf{u}_{n+1} &= \mathbf{u}_n + h\dot{\mathbf{u}}_n + (\frac{1}{2} - \delta)h^2\ddot{\mathbf{u}}_n + \delta h^2\ddot{\mathbf{u}}_{n+1}, \end{aligned} \quad (23)$$

where α and δ are the free parameters of Newmark's method.

For the displacement \mathbf{u}_{n+1} to satisfy the equation (22) at time $t_{n+1} (= t_n + h)$, we can have the incremental equation by applying the Newton method as follows:

$$\mathbf{q}(\mathbf{u}_{n+1}^{k+1}) = \mathbf{q}(\mathbf{u}_{n+1}^k) + \left. \frac{\partial \mathbf{q}}{\partial \mathbf{u}} \right|_{\mathbf{u}_{n+1}^k} \Delta \mathbf{u}_{n+1}^{k+1} = \mathbf{0}, \quad (24)$$

where, $\Delta \mathbf{u}_{n+1}^{k+1}$ is an incremental iterative displacement vector and the tangent iteration matrix, $\partial \mathbf{q} / \partial \mathbf{u}$, is expressed in this non-linear system as

$$\left. \frac{\partial \mathbf{q}}{\partial \mathbf{u}} \right|_{\mathbf{u}_{n+1}^k} = \mathbf{M} \frac{\mathbf{1}}{\delta h^2} + g\mathbf{A}_g \frac{\alpha}{\delta h} + (\mathbf{K}\mathbf{0} + \beta\mathbf{A}_\beta - \mathbf{K}^{AT} + \mathbf{KN1}(\mathbf{u}_{n+1}^k) + \mathbf{KN2}(\mathbf{u}_{n+1}^k)). \quad (25)$$

The updated quantities can be obtained by the corrector equation resulting from equation (23):

$$\begin{aligned} \mathbf{u}_{n+1}^{k+1} &= \mathbf{u}_{n+1}^k + \Delta \mathbf{u}_{n+1}^{k+1}, \\ \ddot{\mathbf{u}}_{n+1}^{k+1} &= \ddot{\mathbf{u}}_{n+1}^k + \frac{\mathbf{1}}{\delta h^2} \Delta \mathbf{u}_{n+1}^{k+1}, \\ \dot{\mathbf{u}}_{n+1}^{k+1} &= \dot{\mathbf{u}}_{n+1}^k + \frac{\alpha}{\delta h} \Delta \mathbf{u}_{n+1}^{k+1}. \end{aligned} \quad (26)$$

For the convergence test, the norms of out-of-balance vector and displacement vector are checked as follows:

$$\|\mathbf{q}_{n+1}^k\| \leq \varepsilon_q \|\mathbf{F}_{n+1} - \mathbf{F}_n\|, \quad \|\Delta \mathbf{u}_{n+1}^{k+1}\| \leq \varepsilon_u \|\mathbf{u}_{n+1}^{k+1}\|. \quad (27)$$

4. RESULTS AND DISCUSSION

4.1. VALIDATION OF FE CODES

Firstly, the linear and non-linear transient responses of unstiffened isotropic and laminated plates are compared with the results of Chen and Sun [12]. The isotropic and laminated square plates with all simply supported boundary conditions are subject to a uniform step loading, \hat{q}_z ; the simply supported boundary conditions are written as

$$\begin{aligned} \text{S.S. on } x\text{-axis: } u = v = w = \phi_x = 0 \quad \text{and} \quad \phi_y \neq 0, \\ \text{S.S. on } y\text{-axis: } u = v = w = \phi_y = 0 \quad \text{and} \quad \phi_x \neq 0. \end{aligned} \quad (28)$$

By using the symmetric characteristics, a quarter of the panel with 9-node 4×4 mesh is modelled. In the Newmark's scheme, $\alpha = 1/2$, $\delta = 1/4$ and $h = 0.002$ s are used. The geometry and material properties of an isotropic plate are given as follows:

$$\begin{aligned} E = 68.9 \text{ GPa}, \nu = 0.25, \rho = 2.496 \times 10^3 \text{ kg/m}^3, \\ a = 23.8 \text{ cm}, c = 0.635 \text{ cm}, \hat{q}_z = 47.84 \text{ Pa} (0 \leq t \leq \infty). \end{aligned} \quad (29)$$

For the verification of composite plates, a $[0/90]_s$ laminated plate is analyzed with the following structural parameters:

$$\begin{aligned} E_1/E_2 = 25, G_{12} = G_{13} = 0.5E_2, G_{23} = 0.2E_2, \\ \nu_{12} = 0.25, E_2 = 1.0, \rho = 1.0, \\ a = 1.0, a/c = 10, a/b = 1, h = \Delta t = 0.1. \end{aligned} \quad (30)$$

The results in Figure 2 show the non-linear transient responses of isotropic and laminated square plates subject to uniform transverse load. Because of geometric non-linearity, both the maximum central deflection and the time period decrease. The present results are in fairly good agreement with the results of Chen and Sun [12] in the linear and non-linear analyses.

Secondly, the limit cycle oscillation of an isotropic square plate with all simply supported boundary conditions, considering a supersonic piston aerodynamic theory, is compared with previous results. A 6×6 mesh with 9-node elements is modelled and $\alpha = 1/2$, $\delta = 1/4$, and $h = 0.0001$ s in the Newmark's scheme are used. The isotropic plate with $\nu = 0.3$ is subject to uniform temperature in all directions. Figure 3 shows that the present results for $\Delta T^* = 0.0, 1.0$ and 2.0 show a very good agreement with previous time integration results by Dowell [1] and Zhou *et al.* [5] using six normal modes.

4.2. DEFINITION OF ANALYSIS MODELS

In this study, linear and non-linear characteristics of the supersonic panel flutter are investigated using both frequency domain and time domain analyses. Figure 1 shows

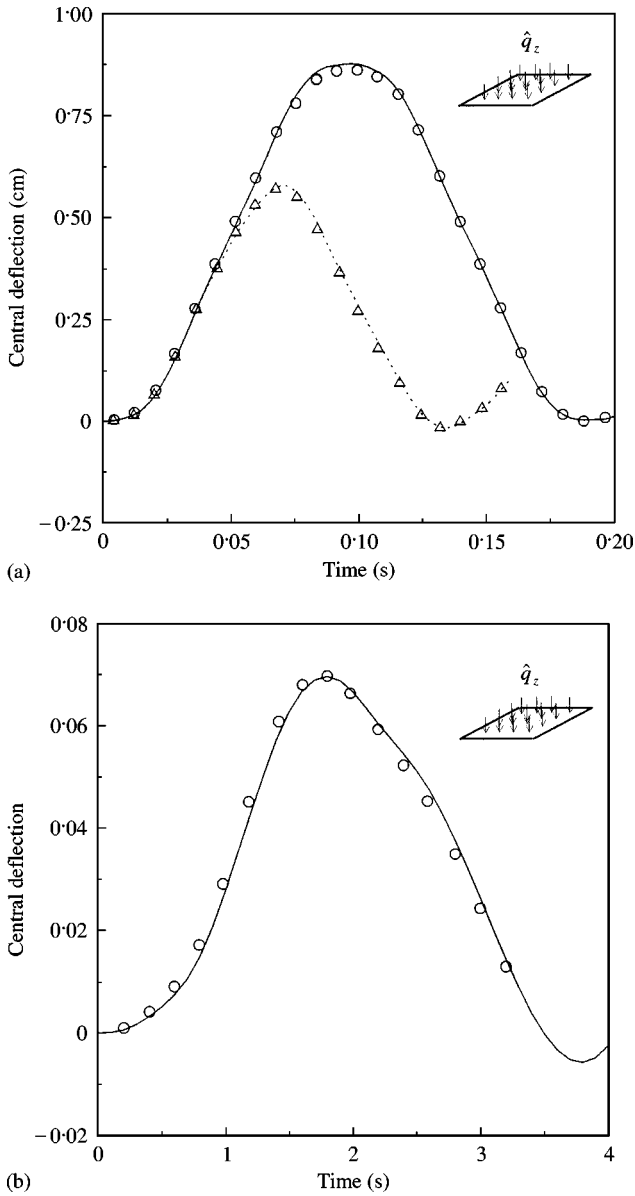


Figure 2. Transient response of square plate subject to uniform transverse load. (a) Isotropic panel: \circ , Chen & Sun (linear); \triangle , Chen & Sun (Nonlinear); —, present (linear); \cdots , present (nonlinear); (b) Composite panel: \circ , Chen & Sun ($[0^\circ/90^\circ]$); —, present ($[0^\circ/90^\circ]$).

a stiffened plate subject to thermal and aerodynamic loads. Material properties and geometry are given as follows:

$$\begin{aligned}
 E_1 &= 206.8 \text{ GPa}, E_2 = 18.2 \text{ GPa}, G_{12} = 5.4 \text{ GPa}, G_{23} = 3.7 \text{ GPa}, \\
 \nu_{12} &= 0.21, \alpha_1 (\times 10^{-6} \text{ m/m/}^\circ\text{C}) = 6.16, \alpha_2 (\times 10^{-6} \text{ m/m/}^\circ\text{C}) = 22.7, \\
 \rho &= 2000 \text{ kg/m}^3, a/b = 1.0, a/c = 75.
 \end{aligned}
 \tag{31}$$

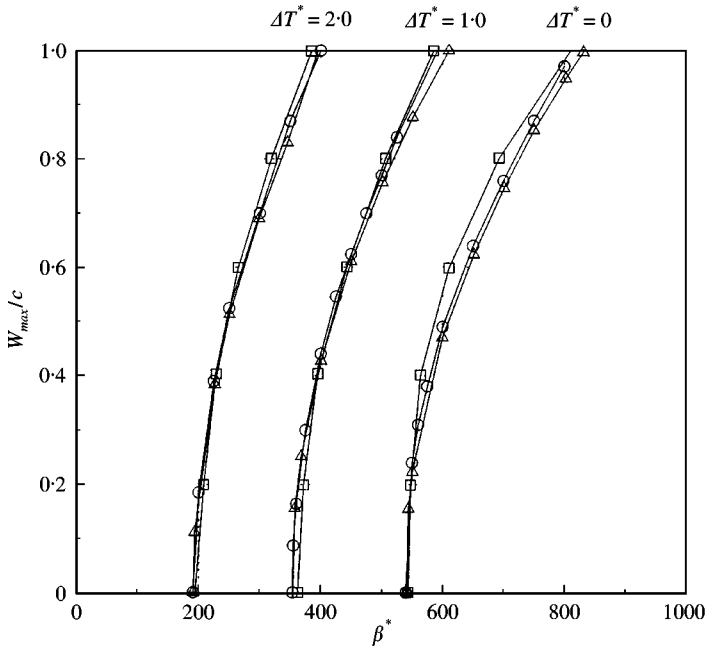


Figure 3. Time domain analysis of limit cycle oscillation for a simply supported isotropic square plate ($\mu/M_\infty = 0.1$): \square —, Dowell; \triangle —, Zhou, Xue, Mei; \circ —, present.

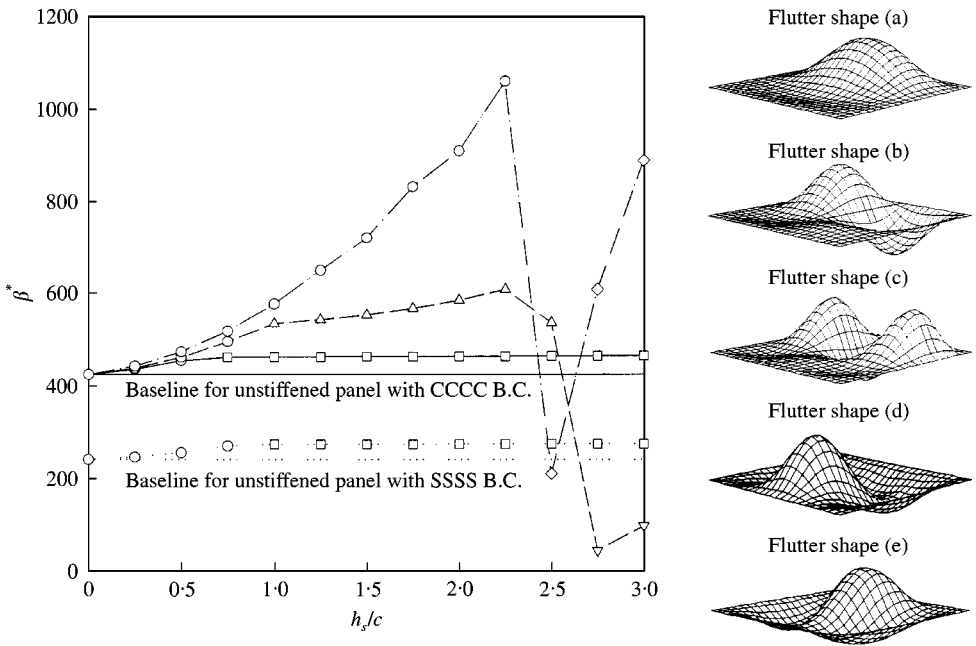

































Figure 4. Effect of stiffener eccentricity on flutter boundary $[(0/90)_2]_s$ square plate with $a/c = 75$: —, panel with 1 stiffener; —, panel with 2 stiffeners; —, panel with 3 stiffeners. Flutter shape: (a) \circ , (b) \square , (c) \triangle , (d) ∇ , (e) \diamond .

TABLE 1

Effect of stiffener height on the vibration and flutter of [(0/90)₂]_s stiffened panels with all clamped boundary conditions

Stiffened [(0/90) ₂] _s composite plate	Without stiffener	With $h_s/c = 0.5$	With $h_s/c = 1.5$	With $h_s/c = 2.5$
				
	$\Delta T_{cr} = 74.53^\circ\text{C}$	$\Delta T_{cr} = 77.80^\circ\text{C}$	$\Delta T_{cr} = 99.32^\circ\text{C}$	$\Delta T_{cr} = 103.89^\circ\text{C}$
First mode				
	$\bar{\omega}_1 = 22.90$	$\bar{\omega}_1 = 23.42$	$\bar{\omega}_1 = 26.34$	$\bar{\omega}_1 = 30.81$
Second mode				
	$\bar{\omega}_2 = 41.33$	$\bar{\omega}_2 = 41.34$	$\bar{\omega}_2 = 41.36$	$\bar{\omega}_2 = 41.38$
Third mode				
	$\bar{\omega}_3 = 51.71$	$\bar{\omega}_3 = 53.24$	$\bar{\omega}_3 = 59.32$	$\bar{\omega}_3 = 63.29$
Fourth mode				
	$\bar{\omega}_4 = 63.19$	$\bar{\omega}_4 = 63.20$	$\bar{\omega}_4 = 63.24$	$\bar{\omega}_4 = 64.72$
Fifth mode				
	$\bar{\omega}_5 = 73.52$	$\bar{\omega}_5 = 73.57$	$\bar{\omega}_5 = 74.24$	$\bar{\omega}_5 = 75.74$
Sixth mode				
	$\bar{\omega}_6 = 88.84$	$\bar{\omega}_6 = 89.53$	$\bar{\omega}_6 = 93.79$	$\bar{\omega}_6 = 101.42$
Flutter mode and dynamic pressure				
Flutter modes				
$\bar{\omega}_{cr}$	44.96	46.35	57.81	57.87
$\beta^*_{flutter}$	424.7	454.6	463.1	464.5

It is well known that the stiffener must be located in the airflow direction to increase a critical dynamic pressure. Hence, it is modelled so that every stiffener is parallel to the airflow and attached to the skin panel with equivalent spacing. In order to enhance the structural performance, the flutter characteristics for structural parameters, such as height (h_s) and number of stiffeners, are primarily investigated. Actually, the dynamic

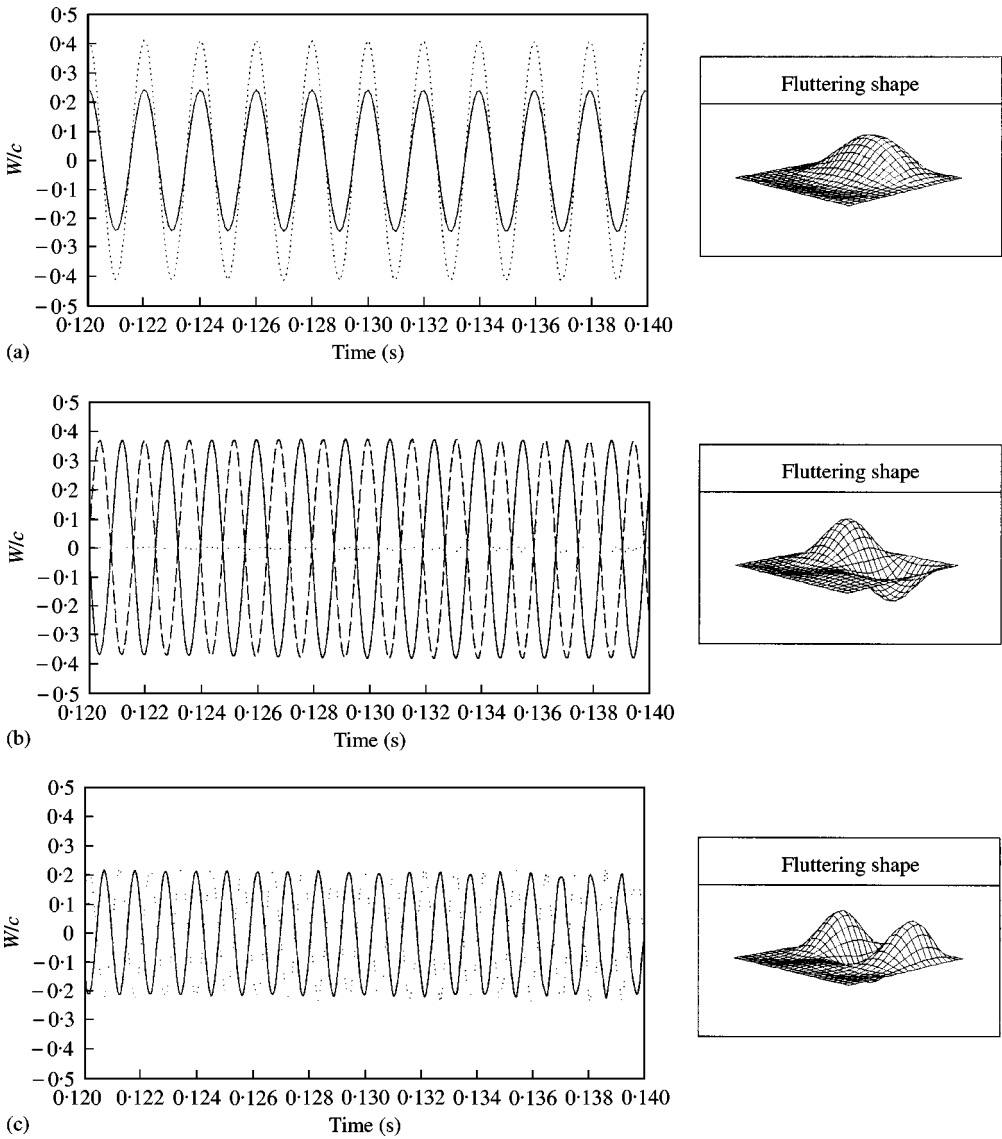


Figure 5. Limit cycle oscillation of stiffened [(0/90)₂]_s panel. (a) One stiffener with $h/c = 0.5$, $\beta^* = 480$; (b) one stiffener with $h/c = 1.5$, $\beta^* = 490$; (c) two stiffeners with $h/c = 1.5$, $\beta^* = 580$. Selection points: —, $\xi = 0.75$, $\eta = 0.25$; , $\xi = 0.75$, $\eta = 0.50$; - - - - - , $\xi = 0.75$, $\eta = 0.75$.

behavior of stiffened laminated plates can be affected by the lamination type and boundary conditions. In this study, cross-ply and quasi-isotropic laminates were analyzed with both simply supported and clamped boundary conditions.

Free vibration and linear flutter analyses considering large deflections are performed in the frequency domain, and non-linear fluttering behaviors beyond the linear flutter boundaries are analyzed in the time domain. In the frequency domain analyses using modal approach, finite elements of stiffened plates are modelled using 9-node 10×12 meshes. In time domain analyses, 9-node 6×6 mesh is fully modelled without using the modal approach. It is assumed that initial deflections are scaled with $\phi_{1max}/c = 0.1$ and initial

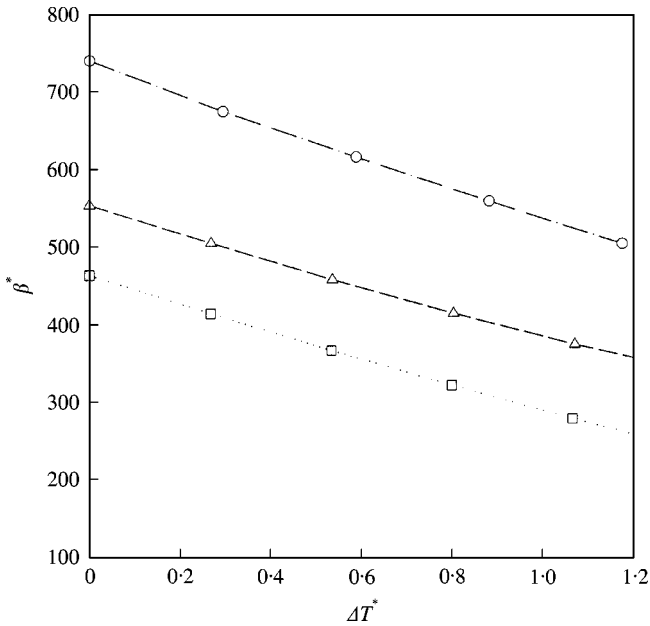


Figure 6. Flutter boundary of $[(0/90)_2]_s$ stiffened composite panel subject to thermal load: —○—, panel with 3 stiffeners: (2, 1) flutter mode; —△—, panel with 2 stiffeners: (2, 3) flutter mode; ---□---, panel with 1 stiffener: (2, 2) flutter mode.

velocities of plates are all zero. Here, a vector, ϕ_1 , is a buckling mode. As an incremental time, $h = 1 \times 10^{-4}$ and 5×10^{-5} s are used for the stiffened plates with one stiffener and two stiffeners respectively. In the supersonic piston theory, an aerodynamic damping factor, μ/M_∞ , is set as 0.01. In the FFT analysis of a steady state time signal, a MATLAB FFT function is used.

4.3. LINEAR FLUTTER CHARACTERISTICS OF STIFFENED PANELS

Linear flutter characteristics of stiffened panels with a $[(0/90)_2]_s$ lamination type are investigated with the variation of the height and number of stiffeners. First, the effects of the height of a stiffener are investigated with $h_s/c = 0.5, 1.5$ and 2.5 . A stiffener is attached to the center of skin plates. Table 1 shows the results for the thermal buckling, free vibration and linear flutter analyses of stiffened plates with one stiffener. As the height of a stiffener increases, the thermal buckling temperature and natural frequencies increase. In case the nodal line of mode shape is located in the position of a stiffener, the variation of natural frequencies for those modes is negligible. As the height of a stiffener increases, the change of natural frequencies for (1, 1) and (2, 1) modes is much larger than that for (1, 2) and (2, 2) modes. In the linear flutter analysis, as the height of a stiffener increases, flutter modes shift from (1, 1) and (2, 1) modes to (1, 2) and (2, 2) modes. In the case of $h_s/c = 1.5$ and 2.5 , because flutter modes are (1, 2) and (2, 2) ones, the increase of a critical aerodynamic pressure is very small. For the stiffened panel with one stiffener, the saturation of the critical dynamic pressure is found above the $h_s/c = 0.75$ in Figure 4.

Secondly, the effect of the stiffener height on the flutter characteristics of stiffened panels with equivalent spacing is studied. Figure 4 shows the trend of the linear flutter boundary of stiffened panels with increasing h_s/c . Results show that if the nodal lines of flutter modes

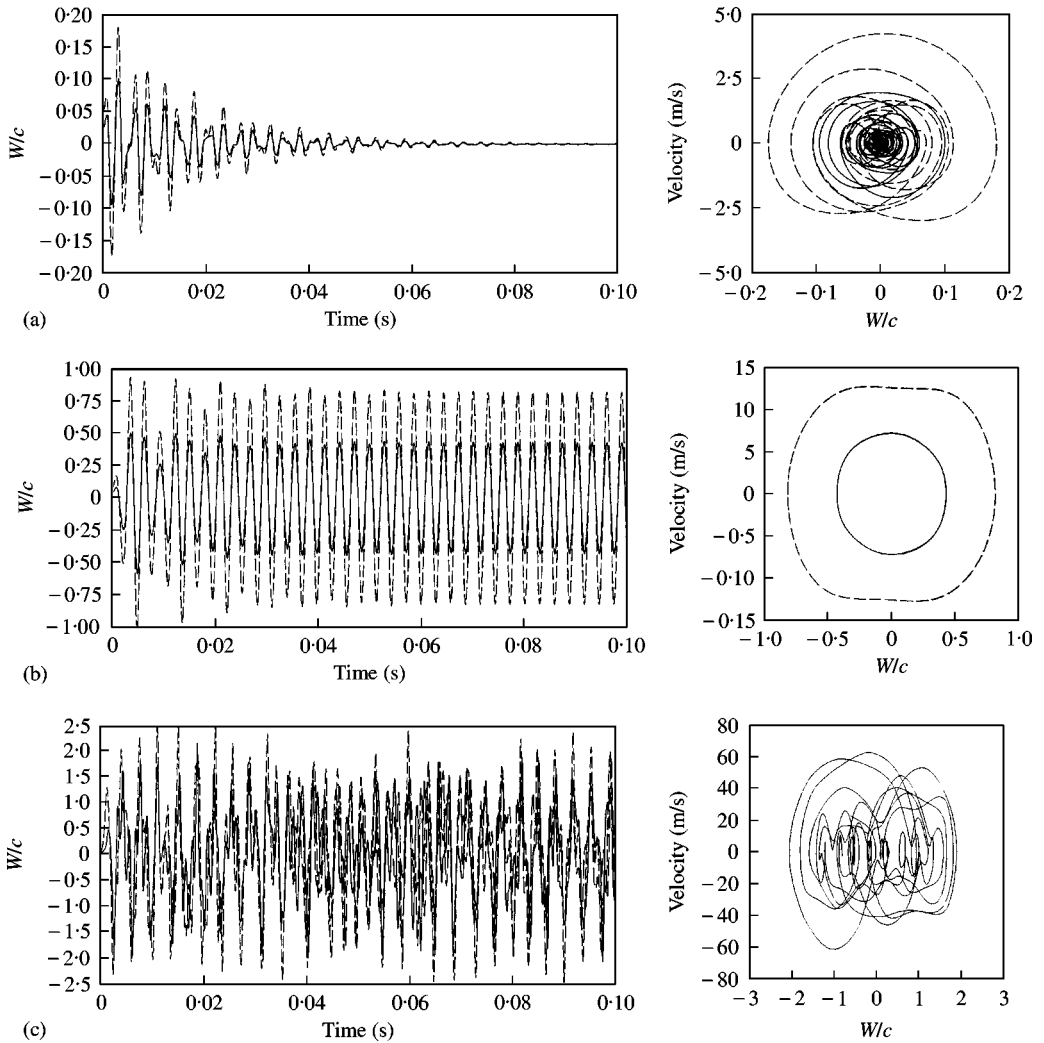


Figure 7. Time history of unstiffened composite panel subject to thermal load. (a) $\Delta T^* = 0.0$, $\beta^* = 300$; (b) $\Delta T^* = 1.2$, $\beta^* = 300$; (c) $\Delta T^* = 3.0$, $\beta^* = 300$: —, $\zeta = 0.75$, $\eta = 0.25$; ---, $\zeta = 0.75$, $\eta = 0.50$; - - - , $\zeta = 0.75$, $\eta = 0.75$.

coincide with the location of stiffener, the increase of the stiffener height to enhance a critical dynamic pressure is not reasonable. The change of flutter modes with increasing h_s/c is found in Figure 4. The results of stiffened panels with two and three stiffeners show the dip of critical dynamic pressures. For the behaviors of stiffened panels with two stiffeners, the flutter modes shift from (a) shape to (c) shape above $h_s/c = 1$ as shown in Figure 4. However, flutter modes change again from (c) shape to (d) shape at a certain region. In the stiffened panels with three stiffeners, flutter modes shift from (a) shape to (e) shape with a dramatic decrease of critical dynamic pressures. It is interesting that owing to the change of flutter mode shape, a dramatic dip in the flutter boundary with increasing h_s/c is found. The difference between the SSSS and CCC boundary conditions in the flutter characteristics is shown in Figure 4. Consequently, in the design of stiffened panels without considering flutter characteristics, an unexpected flutter can occur resulting in structural

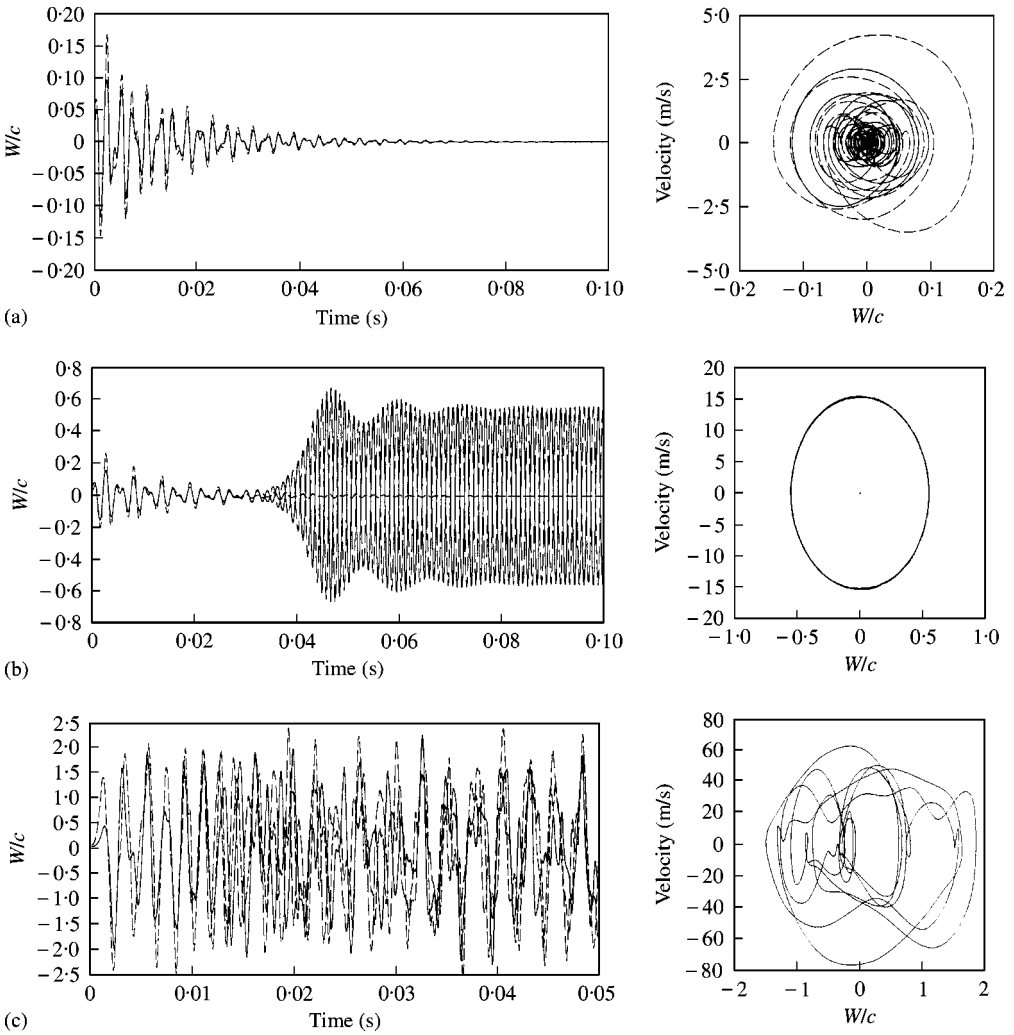


Figure 8. Time history of composite panel with one stiffener subject to thermal load. (a) $\Delta T^* = 0.0$, $\beta^* = 400$; (b) $\Delta T^* = 0.5$, $\beta^* = 400$; (c) $\Delta T^* = 3.0$, $\beta^* = 400$. —, $\zeta = 0.75$, $\eta = 0.25$; ---, $\zeta = 0.75$, $\eta = 0.50$; — —, $\zeta = 0.75$, $\eta = 0.75$.

failure. Also, although the increase of stiffener height can suppress a static deflection, it can abruptly drop the boundaries of a dynamic stability at a certain point.

4.4. NON-LINEAR TRANSIENT ANALYSIS OF STIFFENED PANELS

In addition to linear flutter analysis in a frequency domain, transient non-linear flutter characteristics of stiffened panels are also investigated using a time-integration scheme. It is well known that the limit cycle oscillation without a catastrophic failure occurs after a critical flutter point and results in a fatigue failure of panel structures. The limit cycle oscillation is due to geometrical non-linearity of structures. Also, chaotic oscillations are observed in the panel subject to thermal stresses as well as a severe aerodynamic load. In

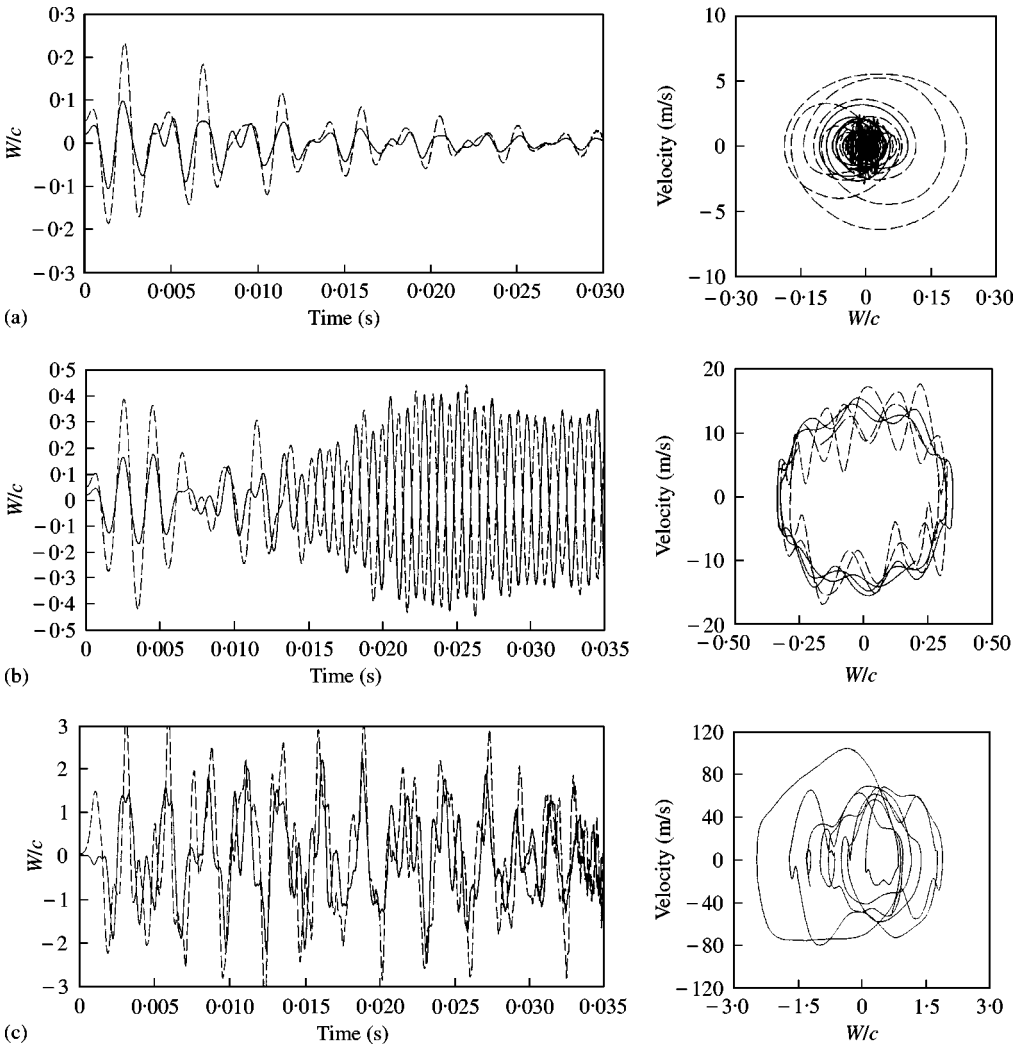










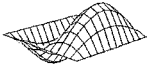



















Figure 9. Time history of composite panel with two stiffeners subject to thermal load. (a) $\Delta T^* = 0.0$, $\beta^* = 500$; (b) $\Delta T^* = 0.5$, $\beta^* = 500$; (c) $\Delta T^* = 3.0$, $\beta^* = 500$: —, $\xi = 0.75$, $\eta = 0.25$; ---, $\xi = 0.75$, $\eta = 0.50$; — —, $\xi = 0.75$, $\eta = 0.75$.

this study, chaotic motions as well as limit cycle oscillations of stiffened panels subject to aero-thermal loads are investigated using a non-linear time-integration scheme.

Firstly, the limit cycle oscillation of stiffened panels with typical fluttering shapes is analyzed. Figure 5 shows limit cycle oscillations of stiffened panels without thermal stresses. Three points on the stiffened panel are selected for the nonlinear transient history as follows: point (a): ($\xi = 3/4$, $\eta = 1/4$), point (b): ($\xi = 3/4$, $\eta = 1/2$), point (c): ($\xi = 3/4$, $\eta = 3/4$).

The non-dimensional parameters are defined as $\xi = x/a$ and $\eta = y/b$. Figure 5(a) shows the limit cycle oscillation of a stiffened panel including one stiffener with $h_s/c = 0.5$. As the height of a stiffener increases, the typical fluttering shape is shown in Figure 5(b). As previously explained, another fluttering shape appears from the mergence of (1, 2) and (2, 2) modes. Figure 5(c) shows the non-linear transient response of stiffened panels with two stiffeners. The fluttering shape shown in Figure 5(c) is due to the location of two stiffeners.

TABLE 2
Effect of stiffener eccentricity on the vibration characteristics of [0/45/ - 45/90]_s stiffened panels with all simply supports

Composite laminated plate	Without stiffener	With 1 stiffener	With 2 stiffeners	With 3 stiffeners
				
	$\Delta T_{cr} = 26.426^\circ\text{C}$	$\Delta T_{cr} = 43.616^\circ\text{C}$	$\Delta T_{cr} = 32.495^\circ\text{C}$	$\Delta T_{cr} = 29.707^\circ\text{C}$
First mode				
	$\bar{\omega}_1 = 12.08$	$\bar{\omega}_1 = 16.08$	$\bar{\omega}_1 = 13.43$	$\bar{\omega}_1 = 12.84$
Second mode				
	$\bar{\omega}_2 = 24.34$	$\bar{\omega}_2 = 24.53$	$\bar{\omega}_2 = 24.97$	$\bar{\omega}_2 = 24.66$
Third mode				
	$\bar{\omega}_3 = 35.98$	$\bar{\omega}_3 = 44.94$	$\bar{\omega}_3 = 42.17$	$\bar{\omega}_3 = 39.69$
Fourth mode				
	$\bar{\omega}_4 = 44.30$	$\bar{\omega}_4 = 46.47$	$\bar{\omega}_4 = 44.79$	$\bar{\omega}_4 = 44.49$
Fifth mode				
	$\bar{\omega}_5 = 48.80$	$\bar{\omega}_5 = 49.14$	$\bar{\omega}_5 = 52.67$	$\bar{\omega}_5 = 51.09$
Sixth mode				
	$\bar{\omega}_6 = 66.77$	$\bar{\omega}_6 = 73.53$	$\bar{\omega}_6 = 66.77$	$\bar{\omega}_6 = 68.10$

Results show that the maximum deflection of points (a) and (b) is nearly the same with 180° phase shift.

Next, flutter characteristics of stiffened panels subject to thermal loads is investigated. It is well known that thermal stresses can lower the flutter stability of panels. Unlike flat panels, static aero-thermal deflections at the flutter point can exist in the stiffened panels.

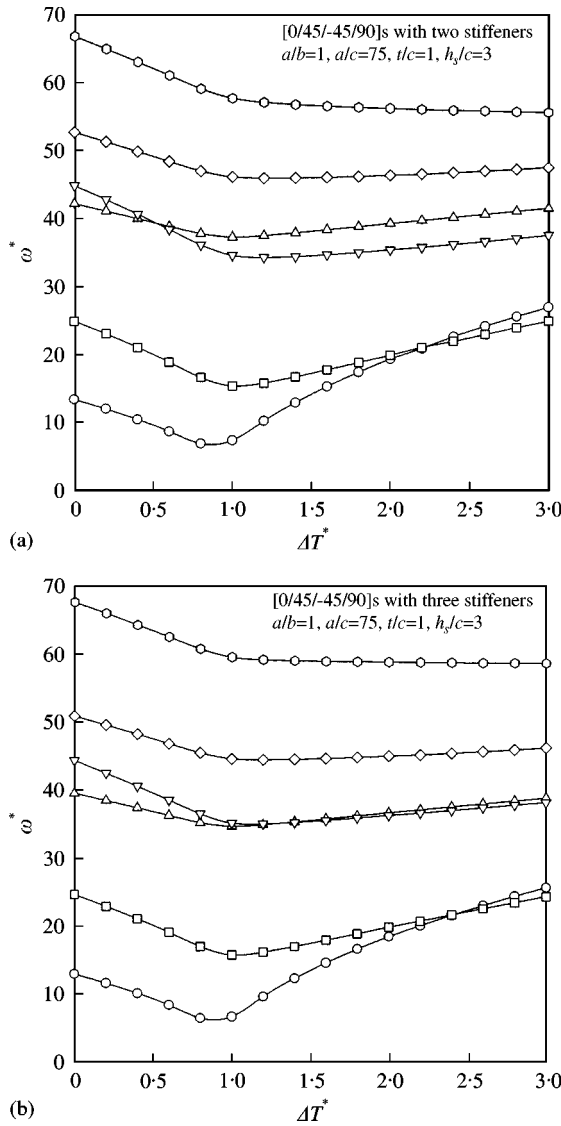


Figure 10. Vibration history of stiffened panels subject to thermal loads with [0/45/ - 45/90]s lamination and all simply supports. (a) Stiffened panel with two stiffeners. (b) stiffened panel with three stiffeners: —○—, first mode; —□—, second mode; —△—, third mode; —▽—, fourth mode; —◇—, fifth mode; —○—, sixth mode.

This is due to the thermal moment from the eccentric effect of stiffeners. Figure 6 shows the linear flutter boundary of stiffened panels subject to thermal loads. In this study, stiffened panels with one, two and three stiffeners are analyzed. As the temperature of panels increases, the critical dynamic pressure decreases. Results indicate that stiffened panels with many stiffeners have a merit for thermal buckling and flutter.

Beyond the linear flutter boundary, non-linear fluttering characteristics such as limit cycle, non-periodic and chaotic motions are investigated in a time domain. Figure 7 shows the transient response of an unstiffened panel with the variation of temperature distribution. Under a critical dynamic pressure, a stable motion is shown in Figure 7(a). But, as the thermal stresses are induced in the panel with increasing ΔT^* , the limit cycle

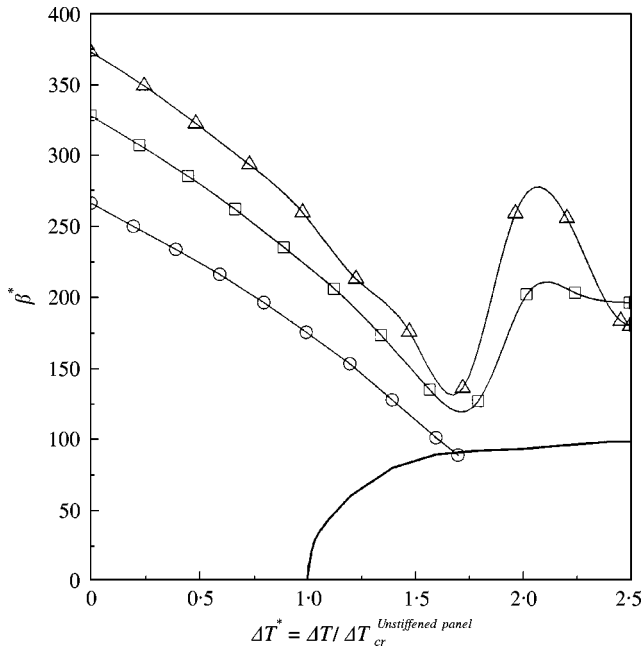


Figure 11. Flutter boundary of stiffened panels subject to thermal loads: —, aerothermal buckling boundary of an unstiffened panel; \circ —, unstiffened panel; \square —, stiffened panel with two stiffeners; \triangle —, stiffened panel with three stiffeners.

oscillation with large amplitude and chaotic motions appears as shown in Figure 7(b) and (c). Figure 8 shows the aerothermoelastic response of a stiffened panel with one stiffener in a time domain. Below a critical dynamic pressure, a dynamically stable motion is also shown in Figure 8(a). When a normalized temperature rises up to 0.5, limit cycle oscillations with fluttering shape from the merge of (1, 2) and (2, 2) modes are shown in Figure 8(b). Chaotic motions also appear with increasing temperature in Figure 8(c). The results of the transient analysis of stiffened panels with two stiffeners are shown in Figure 9.

The effect of the number of stiffeners on the vibration and flutter characteristics is also investigated in the frequency and time domain analyses. The analysis model is given as follows:

Common points.

Lamination: $[0/45/-45/90]_s$.

Boundary conditions: all simply supported,

Geometry: $a/b = 1$, $a/c = 75$, $t/c = 1$,

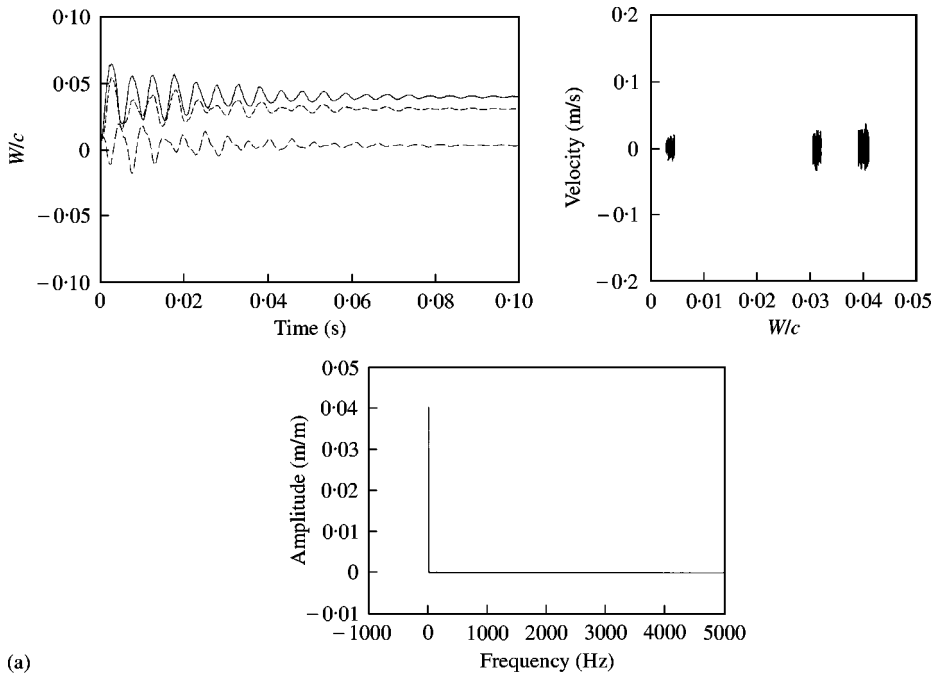
Three models of stiffened panels:

(a) one stiffener with $h_s/c = 3.0$,

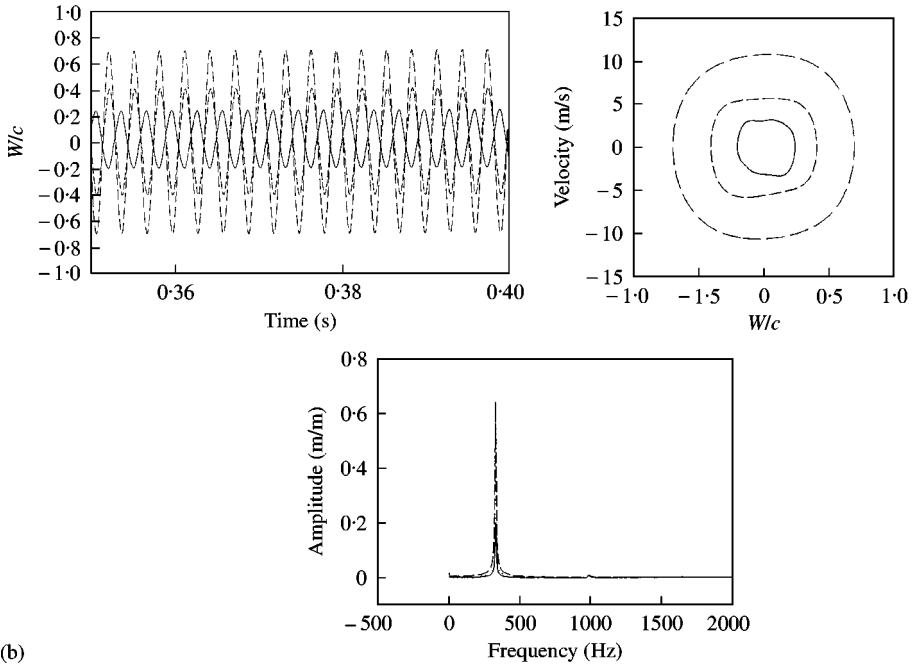
(b) two stiffeners with $h_s/c = 1.5$,

(c) three stiffeners with $h_s/c = 1.0$.

Table 2 shows the thermal buckling temperatures, natural frequencies, and mode shapes of three stiffened panels with the same volume of stiffeners. From the results, the fundamental frequency and thermal buckling temperature of a stiffened panel with one stiffener is the highest. In the mode shapes of the stiffened panel with one stiffener, the (2, 1) mode shape, which is generally a flutter mode, disappeared. Figure 10 shows the vibration history of stiffened panels with two and three stiffeners subject to thermal loads. In the region of $\Delta T^* = 1.0$, natural frequencies have the minimum value. However, the natural

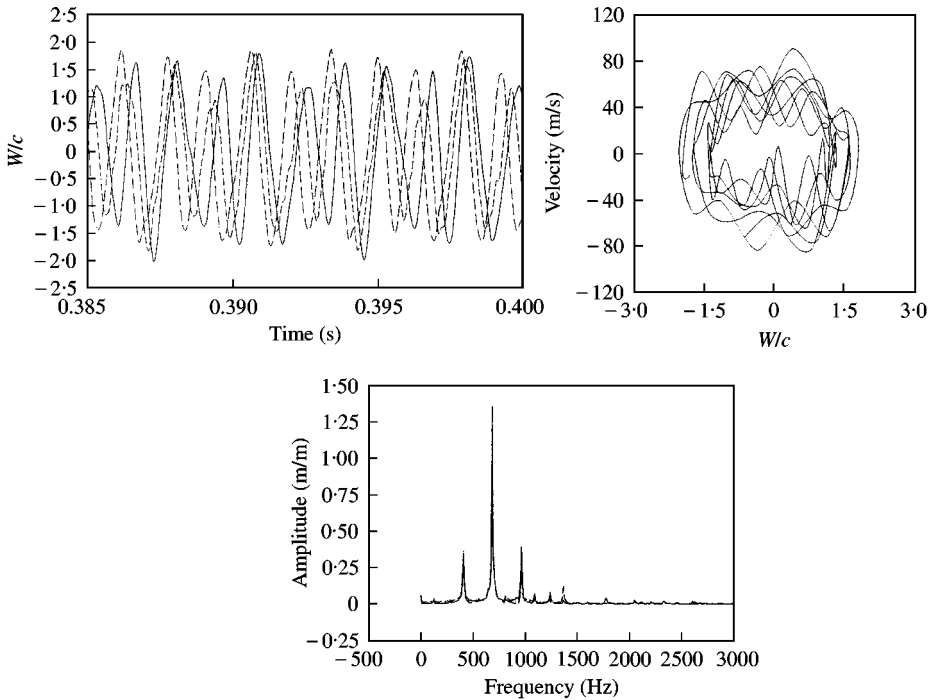


(a)



(b)

Figure 12. Fluttering phenomena of stiffened panels with two stiffeners. (6×6 mesh, 9 node ele.) (a) $\Delta T^* = 1.0$, $\beta^* = 150$; —, ($\xi = 0.75$, $\eta = 0.25$); ---, ($\xi = 0.75$, $\eta = 0.50$); -.-, ($\xi = 0.75$, $\eta = 0.75$). (b) $\Delta T^* = 1.0$, $\beta^* = 300$; (c) $\Delta T^* = 1.0$, $\beta^* = 400$.



(c)

Figure 12. Continued.

frequencies increase again because of geometrical non-linearity. Flutter boundaries of stiffened panels subject to thermal loads are shown in Figure 11. The non-dimensional temperature parameter is normalized as the thermal buckling temperature of an unstiffened panel. The critical dynamic pressure of stiffened panels with three stiffeners is the highest. Generally, as the temperature increases, flutter boundaries of stiffened panels decrease. Figure 12 shows the fluttering response of stiffened panels with two stiffeners. The figure shows results of both time and frequency domains. The dynamically stable motion with static aero-thermal deflections is observed at $\Delta T^* = 1.0$ and $\beta^* = 150$ as shown in Figure 12(a). As the dynamic pressure increases, limit cycle oscillations and periodic motions are also observed as shown in Figure 12(b) and (c).

5. CONCLUSION

In this study, linear and non-linear flutter characteristics of stiffened panels subject to thermal loads are investigated using both frequency domain and time domain analyses. The first order shear deformable plate and Timoshenko beam theories are used for the finite element modelling of a skin panel and stiffeners considering von Karman non-linear strain-displacement relationships. A supersonic piston theory is used for modelling aerodynamic loads.

The effects of the height and number of stiffeners on thermal buckling, vibration and flutter are studied in the frequency domain. In case the nodal line of flutter modes coincides with the location of stiffeners, the variations of natural frequencies and flutter bounds is very

small although the height of stiffeners increases. As the height and number of stiffeners change, the flutter modes can be changed to another shape resulting in the dramatic decrease of the critical dynamic pressure. Although the increase of the stiffener height can suppress a static deflection, it can abruptly drop the boundaries of a dynamic stability at a certain point.

Also, the non-linear behaviors, such as dynamically stable motion with static aero-thermal deflections, limit cycle oscillations, periodic motions with large amplitude and chaotic motions, are observed in the time domain analysis. Since non-linear large-amplitude motions can give a fatigue failure of stiffened panels, the careful analysis of fluttering motions for stiffened panels should precede in the stage of structural design.

REFERENCES

1. E. H. DOWELL 1970 *American Institute of Aeronautics and Astronautics Journal* **8**, 385–399. Panel flutter: a review of the aeroelastic stability of plates and shells.
2. C. C. KUO, L. MORINO and J. DUGUNDJI 1972 *American Institute of Aeronautics and Astronautics Journal* **10**, 1479–1484. Perturbation and harmonic balance methods for nonlinear panel flutter.
3. S. W. YUEN and S. L. LAU 1991 *American Institute of Aeronautics and Astronautics Journal* **29**, 1472–1479. Effects of inplane load on nonlinear panel flutter by incremental harmonic balance method.
4. D. Y. XUE and C. MEI 1993 *American Institute of Aeronautics and Astronautics Journal* **31**, 154–162. Finite element nonlinear panel flutter with arbitrary temperatures in supersonic flow.
5. R. C. ZHOU, D. Y. XUE and C. MEI 1994 *American Institute of Aeronautics and Astronautics Journal* **32**, 2044–2052. Finite element time domain-modal formulation for nonlinear flutter of composite panels.
6. J. F. ABBAS, R. A. IBRAHIM and R. F. GIBSON 1993 *American Institute of Aeronautics and Astronautics Journal* **31**, 1478–1488. Nonlinear flutter of orthotropic composite panel under aerodynamic heating.
7. R. UDRESCU 2000 41st *AIAA/ASME/ASCE/AHS/ASC Structures, Structural Dynamics and Material Conference and Exhibit*, AIAA 2000–1531. On the understanding of snap-through phenomenon in aerothermoelasticity of panels.
8. C. L. LIAO and Y. W. SUN 1993 *American Institute of Aeronautics and Astronautics Journal* **31**, 1897–1905. Flutter analysis of stiffened laminated composite plates and shells in supersonic flow.
9. D. M. LEE and I. LEE 1996 *American Institute of Aeronautics and Astronautics Journal* **34**, 637–639. Supersonic flutter analysis of stiffened isotropic and anisotropic panels.
10. I. LEE, D. M. LEE and I. K. OH 1999 *Journal of Sound and Vibration* **224**, 49–67. Supersonic flutter analysis of stiffened laminated plates subject to thermal load.
11. D. M. LEE and I. LEE 1995 *Computers and Structures* **57**, 99–105. Vibration analysis of anisotropic plates with eccentric stiffeners.
12. J. K. CHEN and C. T. SUN 1985 *Computers and Structures* **21**, 513–520. Nonlinear transient responses of initially stressed composite plates.

APPENDIX A: NOMENCLATURE

a	length of panel along x direction
b	length of panel along y direction
c	thickness of panel along z direction
h_s	height of stiffener
t	thickness of stiffener
e	eccentricity of stiffener
D	rigidity of panel
$\bar{\omega}$	non-dimensional frequency
M	Mach number
β	aerodynamic pressure parameter
β^*	non-dimensional dynamic pressure

q	dynamic pressure
\mathbf{q}	residual vector of force balance
g	aerodynamic damping parameter
α, δ	free parameters of Newmark's scheme
h	incremental time in Newmark's scheme
ΔT^*	non-dimensional temperature
Θ	thermal buckling mode
Φ	vibration mode shape
ε_n	convergence tolerance of displacement criteria
ε_q	convergence tolerance of force criteria
<i>Superscript</i>	
b	stiffener
<i>Subscript</i>	
\cdot^x	derivative with respect to x
\cdot^y	derivative with respect to y